Modeling MTC and HTC Radio Access in a Sliced 5G Base Station

Vincenzo Mancuso[1], Paolo Castagno[2], Matteo Sereno[2], and Marco Ajmone Marsan[1,3]
[1]IMDEA Networks Institute, Madrid, Spain; [2]University of Turin, Italy; [3]Polytechnic of Turin, Italy
vincenzo.mancuso@imdea.org, matteo.sereno@unito.it, paolo.castagno@unito.it, ajmone@polito.it

***Abstract*—In this article, we develop a modeling framework to describe the uplink behavior of radio access in a sliced cell, including most features of the standard 3GPP multiple access procedures. Our model allows evaluating throughput and latency of each slice, as a function of cell parameters, when resources are in part dedicated to individual slices and in part shared. The availability of an accurate model is extremely important for the automated run time management of the cell and for the correct setting of its parameters. Indeed, our model considers most details of the behavior of sliced 5G cells, including Access Class Barring (ACB) and Random Access CHannel (RACH) procedures, preamble decoding, Random Access Response (RAR), and Radio Resource Control (RRC) procedures.**

To cope with a number of slices devoted to serve various co-deployed tenants, we derive a multi-class queueing model of the network processor. We then present (i) an accurate and computationally efficient technique to derive the performance measures of interest using continuous-time Markov chains, which scales up to a few slices only, and (ii) tight performance bounds, which are useful to tackle the case of more than a fistful of slices. We prove the accuracy of the model by comparison against a detailed simulator. Eventually, with our performance evaluation study, we show that our model is very effective in providing insight and guidelines for allocation and management of resources in cells hosting slices for services with different characteristics and performance requirements, such as machine type communications and human type communications.

***Index Terms*—Radio access network; 5G; Base station; Slicing; Queuing networks; HTC and MTC coexistence.**

I. Introduction

Network slicing is a defining feature of the 5G technology. It allows the presence of several tenants on one infrastructure, and the effective coexistence of services with quite different characteristics and requirements in different virtual slices of the same network. The NGMN (Next Generation Mobile Network) Alliance [2], formed by mobile network operators and equipment manufacturers, gives the following definition of *network slice instance* [3]: "a set of network functions, and resources to run these network functions, forming a complete instantiated logical network to meet certain network characteristics required by the service instance(s)." Network slicing is thus based on the allocation of a shared or dedicated portion of the network resources to each slice, to achieve the best possible Quality of Service (QoS) for each slice, expressed by means of the relevant key performance indicators (KPIs) like throughput, latency, service availability, etc. ETSI Technical Specification 123 501 [4] defines three classes of slices. The first class refers to slices "suitable for the handling of 5G enhanced mobile broadband" (eMBB). The second class refers to slices "suitable for the handling of ultra-reliable low latency communications" (URLLC). The third class refers to slices "suitable for the handling of massive IoT" (mIoT). Several slices of the same class can coexist on one infrastructure.

The allocation of resources to the individual slices and their real-time management can be implemented with the support of Software Defined Networking (SDN) and Network Function Virtualization (NFV) approaches, hence with management and orchestration (MANO) functions, and in particular with a resource orchestrator that monitors KPIs on different slices and properly manages resources, so as to avoid Service Level Agreement (SLA) violations.

While several papers already looked at the issues related to resource orchestration (as we discuss in the Related Work Section), in this paper we look at the problem of uplink radio resource allocation to slices on the radio interface of one cell, an issue which, to the best of our knowledge, has not yet been considered in the technical literature[1]. In particular, we develop a detailed stochastic model of the behaviour of the sliced cell radio access, including: (i) Access Class Barring (ACB) techniques, (ii) Random Access CHannel (RACH) procedures, (iii) preamble decoding and Random Access Response (RAR), and (iv) Radio Resouce Control (RRC) procedures.

The development of a model capable of predicting the QoS achieved by services using the different slices available in the cell as a function of the cell parameters is extremely important for the automated run time management of the cell and for the correct setting of its parameters, aiming at the simultaneous fulfillment of SLAs in all slices.

Our model builds on the approach we presented in [5] and extends it to account for the presence of slices. It allows the computation of the throughput achieved by each slice, as well as the distribution of delays for each service in each slice. We focus in particular on the case of HTC (human-type communications) and MTC (machine-type communications), the former including broadband services, while the latter

This work is partially supported by the Region of Madrid through the TAPIR-CM project (S2018/TCS-4496), by a Ramon y Cajal grant (ref: RYC-2014-16285) from the Spanish Ministry of Economy and Competitiveness, and by HOME (Hierarchical Open Manufacturing Europe) project supported by the Regione Piemonte, Italia (framework program POR FESR 14/20). A preliminary version of this work appeared in the proceedings of IEEE Infocom'19 [1].

[1]Except for a preliminary version of this work that appeared in [1],

embraces both time-critical and massive-type services. In both cases we rely on eMBB slices, which are the only suitable type of slice when it comes to handle large numbers of devices active ad the same time [4]. Alternative access schemes, e.g., NOMA-based grant-free access techniques are convenient only for devices generating traffic sporadically [6], while fast uplink grants proactively generated by the base station incur non-negligible delay and packet dropping, and reduce the capacity of the cell [7]. This explains why today one of the key questions about 5G KPIs concerns the possibility of coexistence of eMBB for the provision of an increasingly rich gamut of services to human end users, together with the services required by either massive or critical MTC necessary for implementing smart factory, industry 4.0 and IoT concepts.

Our main contributions are as follows:

- We develop a flexible detailed analytical model for the performance analysis of one cell hosting several slices.
- We provide expressions for the computation of relevant KPIs, such as slice throughput and latency distribution.
- We apply the model to the investigation of the performance of one cell hosting up to six slices for HTC and MTC.
- We provide insight and guidelines for the allocation and management of resources in cells hosting HTC and MTC slices.

The rest of this paper is organized as follows. Section II provides a detailed description of the studied system. Section III presents our analytical model and derives expressions for KPIs. Section IV describes and comments results for the case of two to six MTC/HTC slices, validates them by comparison against simulation, and discusses the main model's insights. Section V positions our work with respect to previous work. Finally, Section VI concludes the paper.

TABLE I
NOTATION USED IN THE ARTICLE

Notation	*Description*	*Notation*	*Description*
$A^{(i)}$	ACB backoff for slice i	$p_R^{(i)}$	RACH failure prob. without collision (slice i)
$B^{(i)}$	RACH backoff for slice i	τ	RAO interval
C	BS capacity	$T_{\min}$	Minimum time needed to get a RACH reply
$C^{(i)}$	BS capacity dedicated to slice i	$T_{\max}$	RACH timeout
C_s	shared BS capacity	$T_O^{(i)}$	application timeout for slice i
$k_{\max}^{(i)}$	max number of RACH attempts (slice i)	$Y_k^{(i)}$	time elapsed when leaving stage k (slice i)
M	max number of RRC_CONNECTED terminals	Z	time spent in a RACH stage waiting for an ACK
$M^{(i)}$	guaranteed RRC_CONNECTED positions (slice i)	$\zeta^{(i)}$	exogenous arrivals for slice i
M_s	shared RRC_CONNECTED places	$\lambda^{(i)}$	RACH request arrivals for slice i
N_p	number of random access preambles	Θ	RACH limit per RAO (slice-oblivious)
$o^{(i)}$	power ramping offset for slice i	$\sigma^{(i)}$	flow of acknowledged RACH requests (slice i)
$p_A^{(i)}$	barring probability for slice i	$\phi^{(i)}$	flow of decoded RACH requests for slice i
p_B	blocking probability (same for all slices)	$\psi^{(i)}$	RACH throughput for slice i
$p_C^{(i)}$	RACH collision probability observed by slice i	$\xi^{(i)}$	Network processor throughput for slice i

II. Slicing Radio Access Resources

Here we describe radio resource sharing among slices, using the notation of Table I.

A. Access and Connection Procedures

All devices that need to access a service, of both MTC and HTC types, must execute the random access procedure, that starts when a RACH (Random Access CHannel) opportunity (RAO) is offered by the BS. Before accessing the RACH, a terminal may be delayed by the ACB (Access Class Barring) procedure, that allows a prioritization in the RACH access. Barring a service request of a service class happens with a given probability.

The RACH procedure consists in a packet handshake to synchronize BS and terminal and to assign a unique identifier to the terminal service request. A request is successful only when resources are actually allocated to the terminal with the signaling messages that are exchanged after the random access success. Indeed, the standard 3GPP access procedure includes the RACH access phase and the RRC (Radio Resource Control) connect phase, with four messages exchanged in total. In case of failure during one of the two stages, the terminal repeats its attempt after a random backoff delay, possibly with different transmission power, according to the standard 3GPP power ramping mechanism that defines how nodes progressively increase their transmission power after each failed attempt [8]. Different backoff values can be defined for failures in different points of the procedure.

In the RACH access phase, the terminal chooses one out of N_p available preambles, and transmits it at the next available RAO. If several terminals choose the same preamble, a collision occurs, and the access request cannot be decoded. Note that this is a conservative assumption, since decoding could happen for the highest power transmission in some cases, due to the radio capture effect; our analysis is thus slightly pessimistic. If just one terminal chooses a given preamble, its request is decoded, provided the terminal transmission power is high enough. If a collision occurs, or the power is too low, the RACH access must be repeated.

If a request is decoded, the terminal can receive an acknowledgment from the BS. There is a limit (denoted by Θ in this article) to the maximum number of ACKs that can be transmitted by the BS for each RAO, so that a decoded request can receive no ACK if the limit is reached. If no ACK is received, the terminal must repeat the RACH access procedure.

Terminals that complete the access procedure can move to the RRC_CONNECTED state and receive service from the BS. A limit exists to the maximum number of terminals that

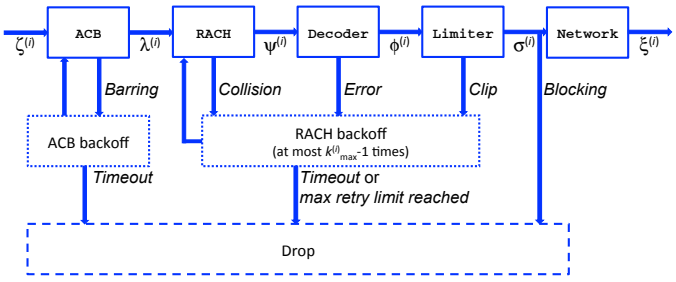

Fig. 1. System blocks representing sliced network functions for the i-th slice hosted by a base station

can be in the RRC_CONNECTED state (we call it M), so that there is a possibility that the terminal request is blocked even after receiving an ACK. In this case, the terminal notifies the user with an error message equivalent to the *busy tone* in the voice phone system.

A maximum number of repetitions for the RACH access procedure is defined, called $k_{\max}$, After $k_{\max}$ attempts, a request is dropped. A repetition can be due to collision (with probability p_C) and to no ACK received (with probability $p_R(k)$ at the k-th attempt, with the associated power level). In addition, a maximum amount of time is defined for the completion of an access procedure instance. When this time is reached, a timeout expires, and the instance is dropped.

Once a terminal is in the RRC_CONNECTED state, it receives its share of the BS capacity, in terms of allocated resource blocks.

This whole procedure is illustrated in Fig. 1, where we see new service request generation on the left, the `ACB` subsystem, followed by the `RACH`, the `Decoder` and the `Limiter`, all with their backoffs, timeout possibilities and maximum number of retries. The `Network` subsystem corresponds to service by the BS, if no blocking occurs. In the system, the following events lead to drop the connection attempt: network blocking, timeout, and exceeding the RACH retry limit.

B. Sliced System

In case of a sliced system, it is necessary to define an allocation of the BS resources to the different slices (identified in this paper with a superscript denoting the slice index).

In the spirit of the 3GPP LTE standard, we assume that the barring probability is a characteristic of a service, but since we allocate one service to each slice, the barring probability $p_A^{(i)}$ depends on the slice. The power ramping offset can provide a significant differentiation among slices, increasing the probability of decoding for the slices using higher power. For this reason we will consider different values for different slices. The subset of RACH preambles that can be used by a slice significantly impacts the collision probability. We will thus consider the case of different subsets (possibly with non-empty intersection) of preambles for different slices. We will instead assume that the ACKs provided by the BS to service requests that succeed on the RACH and at the decoder are equally available to all slices. Obviously, the maximum number of terminals in the RRC_CONNECTED state is a key aspect for governing the slice KPIs, and we will thus consider cases where values are different for different slices. These values have an impact on the bandwidth share obtained by each terminal. Specifically, we assume that the BS allocates portions of bandwidth to each slice, and that the bandwidth is then equally shared within the slice among terminals in the RRC_CONNECTED state. Out of the M available positions, we reserve $M^{(i)}$ for unique use of slice i, with the sum of the $M^{(i)}$ less or equal to M. The remaining positions are shared by all slices. The values of backoff delays and access timeouts must be tailored to the types of service and the KPI goals of each slice, so they must be carefully set by the operator.

Note that we consider a partial isolation of slide resources, and we will show in the Numerical Results Section that this approach can provide better performance with respect to a full isolation.

III. Analysis

We model a sliced system that represents the uplink chain that goes from the end user terminal, to the radio connection to the BS, to network service within a cell. We leave out of the analysis the connection from the BS to the core network and study in detail BS resource slicing.

A. System Flows

The reference system is the one illustrated in Fig. 1, which includes the network procedures described in the previous section. As shown in the figure, each block can either promote a connection request to the next level, until service is completed, or yield a failure event. The figure only indicates flows and some configuration parameters for slice i, although we assume the presence of S slices.

The `ACB` block sees a flow $\zeta^{(i)}$ as input. Barring at the ACB happens with probability $p_A^{(i)}$ and yields backoffs $A^{(i)}$ for slice i, with no limit on the number of consecutive backoffs (up to the timeout values). We assume that, within a slice, ACB backoff durations are i.i.d. and exponentially distributed.

The `RACH` block receives the flow $\lambda^{(i)}$ from the ACB, which is no higher than $\zeta^{(i)}$ due to the possibility of timeout in the ACB. Failures on a RACH access attempt can be due to collision, decoding errors or clipping at `Limiter`. A user cannot distinguish which type of failure occurred, it simply observes that the BS does not acknowledge its request in an interval $T_{\max}$ and then it schedules a RACH backoff before another attempt will start (if the timeout has not expired). We call *stage* k the k-th RACH access attempt. We assume that the RACH backoff durations $B^{(i)}$ are i.i.d. random variables (r.v.'s) with exponential distribution. Each RACH stage k produces a flow $\psi_k^{(i)}$ of successes, which feeds `Decoder`. Of course, the total flow of successes leaving `RACH` is $\psi^{(i)} = \sum_{k=1}^{k_{\max}^{(i)}} \psi_k^{(i)}$.

The `Decoder` block introduces losses based on a decoding probability that depends on the RACH stage, because of power ramping (with specific per-slice offset). The output of `Decoder` is a flow $\phi^{(i)} \leq \psi^{(i)}$, which feeds `Limiter`.

The `Limiter` block causes failures due to the cap Θ on the number of RACH acknowledgments per RAO. This is a hard limit for the ensemble of slices running on the same BS.

The output of `Limiter` is a set of flows $\sigma^{(i)}$, one per slice, such that $\sum_{i=1}^{S} \sigma^{(i)} \leq \Theta/\tau$.

If a service request eventually reaches `Network`, it can still be blocked if the BS network processor has no position left for that slice (and in the shared pool). Blocking happens with probability $p_B^{(i)}$. Conversely, successful requests are served by the network, with a per-slice throughput denoted by $\xi^{(i)} = (1-p_B^{(i)})\sigma^{(i)}$.

The *busy tone* can therefore be caused by network blocking as well as excessive RACH access attempts (after $k_{\max}^{(i)}$ back-to-back RACH failures) or by specific application timeouts (the app running on the terminal and trying to send a message will not wait forever). The *busy tone* is directly returned to the user as the service request is dropped.

For the framework described above, we now derive expressions for the flows (loads and throughputs) and for the distribution of time spent in the system.

B. Access Time

Let us consider a request from slice i that arrives at `ACB`. We denote by $Y_{k-1}^{(i)}$ the time spent by that request from its arrival to ACB to the moment it enters stage k. $Y_{k-1}^{(i)}$ consists of a random number $L^{(i)}$ of barring backoffs, $(k-1)$ times the interval $T_{\max}$ and $k-1$ RACH backoffs.

If there is a success at the k-th stage, the time spent by the request before leaving is $Y_{k-1}^{(i)} + Z$, where the random interval $Z \leq T_{\max}$ is needed to model the delay between RACH request and network grant and it is independent from all r.v.'s $Y_j^{(i)}$, $j = 1, 2, \ldots, k_{\max}^{(i)}$, $i = 1, 2, \ldots, S$. In this case, the request is served with probability $1 - p_B^{(i)}$ or otherwise dropped. Therefore the time spent for a network blocking is the same as for a success (because we are not counting the network service in the access time).

If there is a failure due to the maximum number of RACH attempts, the time spent is $Y_{k_{\max}^{(i)}}^{(i)}$ and the request is dropped. Instead, in case of timeout, the time spent is the timeout value selected for slice i, namely $T_O^{(i)}$, and the request is dropped as well. The distribution of $Y_k^{(i)}$ is

$$F_{Y_k^{(i)}}(x) = \Pr\left\{ \sum_{n=1}^{L^{(i)}} A_n^{(i)} + kT_{\max} + \sum_{n=1}^{k} B_n^{(i)} \leq x \right\}, \quad (1)$$

where $L^{(i)} \geq 0$ is the random number of back-to-back deferrals experienced because of ACB, due to the barring probability $p_A^{(i)}$ associated to slice i, and the subscript n indicates the n-th passage through either the backoff of `ACB` or `RACH`. Similarly, the distribution of $Y_{k-1}^{(i)} + Z$ is

$$F_{Y_{k-1}^{(i)}+Z}(x) = \Pr\left\{ \sum_{n=1}^{L^{(i)}} A_n^{(i)} + (k-1)T_{\max} + \sum_{n=1}^{k-1} B_n^{(i)} + Z \leq x \right\} \quad (2)$$

Because of the independence of the r.v.'s used in the above expressions, denoting by f_Z the p.d.f. of Z, the following useful result holds:

$$F_{Y_{k-1}^{(i)}+Z} = F_{Y_{k-1}^{(i)}} * f_Z. \quad (3)$$

Moreover, the sum of a fixed number of exponential RACH backoffs is an Erlang r.v., and the sum of a geometrically distributed number of ACB exponential backoffs with ACB backoff probability $p_A^{(i)}$ and average ACB backoff $E[A]$ exhibits the following cumulative distribution:

$$\Pr\left\{ \sum_{n=1}^{L^{(i)}} A_n^{(i)} \leq x \right\} = 1 - p_A^{(i)} e^{-\left(1-p_A^{(i)}\right)\frac{x}{E[A]}}, \quad \forall x \geq 0. \quad (4)$$

The above considerations tell that the distribution (1) can be obtained as the convolution of (4) with an Erlang distribution with shape parameter equal to k and average $k\,E[B^{(i)}]$ (i.e., the average of k backoff intervals), and a time shift $k\,T_{\max}$.

C. RACH Stages

A request enters RACH stage 1 if its timeout does not expire during the ACB backoffs. We denote such probability as $P_N^{(i)}(1)$, which is computed through (4) evaluated at $x = T_O^{(i)}$.

Subsequently, and while the timeout does not expire, a request leaves the RACH stage with either a success, or progress to the next stage upon a collision, or a failure in `Decoder` or in `Limiter`. We indicate the probability to access stage k as $P_N^{(i)}(k)$, for which we derive the following recursive expression:

$$P_N^{(i)}(k+1) = P_N^{(i)}(k)\left[1 - \left(1-p_C^{(i)}\right)\left(1-p_R^{(i)}(k)\right)\right] F_{Y_k^{(i)}}(T_O^{(i)}). \quad (5)$$

In the above expression, $p_C^{(i)}$ indicates the collision probability in `RACH`, $p_R^{(i)}(k)$ is the probability of failure in either `Decoder` or `Limiter` in stage k, and $F_{Y_k^{(i)}}(T_O^{(i)})$ is the probability that a timeout does not occur before the end of the backoff of stage k. We will derive such quantities later in this section. Before that, we need to derive the general expressions for the probabilities of the following events to occur: excess RACH retries, success, blocking, and timeout. Those events fully characterize the success of the access attempt.

D. Event Probabilities

RACH retry limit exceeded. The quantity $P_N^{(i)}\left(k_{\max}^{(i)}+1\right)$, formally defined as for other values of k in (5), represents the fraction of $\zeta^{(i)}$ that exceeds the RACH retry limit.

Access attempt success. The fraction of $\zeta^{(i)}$ that observes a success in stage k is derived as the fraction of requests that enters stage k and experiences no failure:

$$P_S^{(i)}(k) = P_N^{(i)}(k)\left(1-p_C^{(i)}\right)\left(1-p_R^{(i)}(k)\right)\left(1-p_B^{(i)}\right) F_{Y_{k-1}^{(i)}+Z}(T_O^{(i)}). \quad (6)$$

The total success probability of slice i, i.e., the fraction of $\zeta(i)$ requests that succeeds, is therefore $P_S^{(i)} = \sum_{k=1}^{k_{\max}^{(i)}} P_S^{(i)}(k)$.

Network blocking. This is similar to the case of success in stage k, but with a network blocking failure:

$$P_B^{(i)}(k) = P_N^{(i)}(k)\left(1-p_C^{(i)}\right)\left(1-p_R^{(i)}(k)\right) p_B^{(i)}\, F_{Y_{k-1}^{(i)}+Z}(T_O^{(i)}). \quad (7)$$

The fraction of access requests $\zeta^{(i)}$ that experiences network blocking is thus $P_B^{(i)} = \sum_{k=1}^{k_{\max}^{(i)}} P_B^{(i)}(k)$.

Timeout. A timeout can occur either during ACB backoffs, with probability $P_{TO}^{(i)}(0) = 1 - P_N^{(i)}(1)$, or during RACH operations. In the k-th stage, a fraction of requests suffer a timeout while waiting for the network grant or during the backoff. Hence, for $k \geq 1$:

$$P_{TO}^{(i)}(k) = P_N^{(i)}(k)\Big\{\Big(1-p_C^{(i)}\Big)\Big(1-p_R^{(i)}(k)\Big)\Big[1-F_{Y_{k-1}^{(i)}+Z}(T_O^{(i)})\Big] + \Big[1-\Big(1-p_C^{(i)}\Big)\Big(1-p_R^{(i)}(k)\Big)\Big]\Big[1-F_{Y_k^{(i)}}(T_O^{(i)})\Big]\Big\}. \tag{8}$$

The total timeout probability observed by a slice is therefore

$$P_{TO}^{(i)} = \sum_{k=0}^{k_{\max}^{(i)}} P_{TO}^{(i)}(k); \tag{9}$$

Busy tone. Access requests that exceed the RACH retry limit, experience a network blocking event, or a timeout, are dropped. Therefore, the busy tone is sent with probability $1 - P_S^{(i)} = P_N^{(i)}\left(k_{\max}^{(i)}+1\right) + P_B^{(i)} + P_{TO}^{(i)}$.

E. Derivation of throughputs and loads with cycles

With the expressions derived so far, we have characterized the trajectory of the exogenous access requests that feed the system for slice i, i.e., $\zeta^{(i)}$. However, the expressions derived are functions of three parameters that we need to derive next: $p_C^{(i)}$, $p_R^{(i)}(k)$, and $p_B^{(i)}$.

RACH collision probability and throughput. The input of `RACH` is the flow $\lambda^{(i)}$ that arrives from `ACB`. However, `RACH` has internal cycles, and $\lambda^{(i)}$ is just the input to the first stage. With the definitions of Section III-C, we have the following input flows for each successive stage (note that $\lambda_1^{(i)} = \lambda^{(i)}$):

$$\lambda_k^{(i)} = \zeta^{(i)} P_N^{(i)}(k), \quad k = 1, 2, \ldots k_{\max}^{(i)}. \tag{10}$$

We model `RACH` as a slotted Aloha system with multiple channels. The load of the system is the sum of the requests arriving to the various stages, whereas the number of channels is the number of preambles assigned by the BS to the slice.

Specifically, each slice receives a set of $N^{(i)}$ dedicated preambles. In addition, the BS keeps a pool of N_s shared preambles that can be accessed by all slices. The total number of preambles is $N_p = N_s + \sum_{i=1}^{S} N^{(i)}$.

In each RACH attempt, according to the standard, a terminal selects a preamble uniformly at random, so that the per-preamble RACH load generated by slice i is

$$\ell^{(i)} = \frac{\zeta^{(i)}}{N^{(i)} + N_s} \sum_{k=1}^{k_{\max}^{(i)}} P_N^{(i)}(k). \tag{11}$$

The collision probability over a single preamble j, from slotted Aloha results with slots of duration τ, is as follows:

$$p_{C,j} = \begin{cases} 1 - e^{-\tau \ell^{(i)}}, \ 1 \leq i \leq S, & \text{dedicated preamble;} \\ 1 - e^{-\tau \sum_{i=1}^{S} \ell^{(i)}}, & \text{shared preamble.} \end{cases} \tag{12}$$

The resulting per-slice RACH collision probability is derived as the average of (12) over the preambles used by a slice and selected uniformly at random at each attempt:

$$p_C^{(i)} = 1 - \frac{N^{(i)} e^{-\tau \ell^{(i)}} + N_s \, e^{-\tau \sum_{q=1}^{S} \ell^{(q)}}}{N^{(i)} + N_s}. \tag{13}$$

The throughput of `RACH` (for slice i and stage k) is:

$$\psi_k^{(i)} = \left(1 - p_C^{(i)}\right) \lambda_k^{(i)}, \quad \psi^{(i)} = \sum_{k=1}^{k_{\max}^{(i)}} \psi_k^{(i)}. \tag{14}$$

Throughput of `Decoder`. At each stage of the RACH, `Decoder` has a different failure probability, due to power ramping in RACH message transmissions [8]. In particular, as explained in [8], the `Decoder` failure probability is expressed as a negative exponential of the power level index (an integer starting from 1 and incremented at each RACH access) used for the transmission. This is the negative exponential of the number of attempts under standard operations, while in our case the expression becomes $e^{-k-o^{(i)}}$, where k is the RACH attempt stage and $o^{(i)} \geq 0$ is an integer representing the slice offset, i.e., the number of steps in the power ramping procedure which are skipped by slice i. Therefore, at stage k, slice i observes the following `Decoder` throughput:

$$\phi_k^{(i)} = \psi_k^{(i)} \left(1 - e^{-\left(k+o^{(i)}\right)}\right) \tag{15}$$

which sums up to a flow $\phi^{(i)} = \sum_{k=1}^{k_{\max}^{(i)}} \phi_k^{(i)}$.

Losses due to `Limiter`. The BS can only grant Θ requests per RAO, shared between the slices. Therefore there are losses when the output of `Decoder` in a RAO interval is higher than Θ requests. With the RACH preamble partition described above, we can compute the distribution of successes per RAO and hence compute the average loss due to `Limiter`.

In a pool of W preambles subject to homogeneous per-preamble load—e.g., in a pool of shared preambles, or in a pool of preambles dedicated to a single slice—the probability ω_a to have exactly a decoded messages in a RAO is approximated with the probability of having a successes over W i.i.d. Bernoulli experiments (one per RACH preamble, which can only output no or one decoded request). The success probability of each Bernoulli experiment is computed from the aggregate number of messages decoded in an interval τ, as shown next.

For a pool of dedicated preambles $N^{(i)}$, the collision probability is the same for all preambles and it is given by (12). Thus, for each preamble, the average output per RAO, after decoding, is

$$p^{(i)} = \tau e^{-\tau \ell^{(i)}} \sum_{k=1}^{k_{\max}^{(i)}} \left(1 - e^{-\left(k+o^{(i)}\right)}\right) \frac{\lambda_k^{(i)}}{N^{(i)} + N_s}, \tag{16}$$

which can be regarded as the Bernoulli success probability of dedicated preambles. For the shared pool, the result is similar:

$$p_s = \tau e^{-\tau \sum_{i=1}^{S} \ell^{(i)}} \sum_{i=1}^{S} \sum_{k=1}^{k_{\max}^{(i)}} \left(1 - e^{-\left(k+o^{(i)}\right)}\right) \frac{\lambda_k^{(i)}}{N^{(i)} + N_s}. \tag{17}$$

For a dedicated pool we have the following distribution:

$$\omega_a^{(i)} = \begin{cases} \binom{N^{(i)}}{a} \left(p^{(i)}\right)^a \left(1-p^{(i)}\right)^{N^{(i)}-a}, & a \in \{0,..,N^{(i)}\}; \\ 0, & \text{otherwise;} \end{cases} \quad (18)$$

while for the shared pool of preambles we have

$$\omega_{sa} = \begin{cases} \binom{N_s}{a} (p_s)^a (1-p_s)^{N_s-a}, & a \in \{0,..,N_s\} \\ 0, & \text{otherwise.} \end{cases} \quad (19)$$

Finally, putting together the different pools, the probability Ω_a to have exactly a messages decoded (from any slice) is

$$\Omega_a = \sum_{a_1=0}^{N_p} \sum_{a_2=0}^{N_p} \cdots \sum_{a_S=0}^{N_p} \omega_{a_1}^{(1)} \omega_{a_2}^{(2)} \cdots \omega_{a_S}^{(S)} \omega_{s(a-\sum_{r=1}^{S} a_r)}. \quad (20)$$

Overall, the average number of losses is

$$E[N_L] = \sum_{a=\Theta+1}^{N_p} (a-\Theta)\,\Omega_a, \quad (21)$$

and we can assume that losses are spread over slices proportionally to their load at `Limiter`:

$$E\left[N_L^{(i)}\right] = E[N_L] \frac{\phi^{(i)}}{\sum_{q=1}^{S} \phi^{(q)}}; \quad (22)$$

The resulting per-slice `Limiter` throughput is

$$\sigma^{(i)} = \phi^{(i)} - \frac{E\left[N_L^{(i)}\right]}{\tau} = \phi^{(i)} \left(1 - \frac{E[N_L]}{\tau \sum_{q=1}^{S} \phi^{(q)}}\right). \quad (23)$$

Since losses at `Limiter` do not discriminate between RACH stages, the `Limiter` throughput per-stage, $\sigma_k^{(i)}$, is obtained by replacing $\phi_k^{(i)}$ for $\phi^{(i)}$ in (23).

Computation of $p_R^{(i)}(k)$. This quantity is the aggregate loss rate due to the combined action of `Decoder` and `Limiter` for requests at stage k:

$$p_R^{(i)}(k) = 1 - \frac{\sigma_k^{(i)}}{\psi_k^{(i)}} = 1 - \left(1 - e^{-\left(k+o^{(i)}\right)}\right)\left(1 - \frac{E\left[N_L^{(i)}\right]}{\tau \phi^{(i)}}\right). \quad (24)$$

F. A model for the `Network` subsystem in a Sliced BS

The `Network` subsystem is a BS network processor. It can serve at most M users at the same time, and the M available positions in service must be shared among slices. Each slice is granted exclusive access to $M^{(i)}, i = 1, 2, \cdots, S$ positions, with $\sum_{i=1}^{S} M^{(i)} = M - M_s$, and $M_s \geq 0$. If not all positions are dedicated (i.e., $M_s > 0$), remaining positions are shared among all slices. Arrivals that do not find available service positions are dropped, thus originating the network blocking probability.

The `Network` subsystem has total service capacity C services per second, out of which $C^{(i)}, i = 1, 2, \cdots, S$, is reserved for slice i, and C_s is shared among slices. If `Network` is serving up to $M^{(i)}$ users for slice i, they equally share $C^{(i)}$. However, when there are $m^{(i)} > M^{(i)}$ customers, the i-th queue obtains a service rate equal to $C^{(i)}$ plus a portion of the shared capacity C_s proportional to $m^{(i)} - M^{(i)}$. Hence, the i-th queue service rate depends on the total number of services of all slices, i.e., the service rate when $m^{(i)} > M^{(i)}$ is $C_i + C_s / \sum_{i=1}^{S} \max\left(0, m^{(i)} - M^{(i)}\right)$. This service policy is reasonable when most of resources are dedicated to slices, and the fraction of shared capacity is small. Other policies can be considered in different scenarios, and studied with approaches similar to what we describe below.

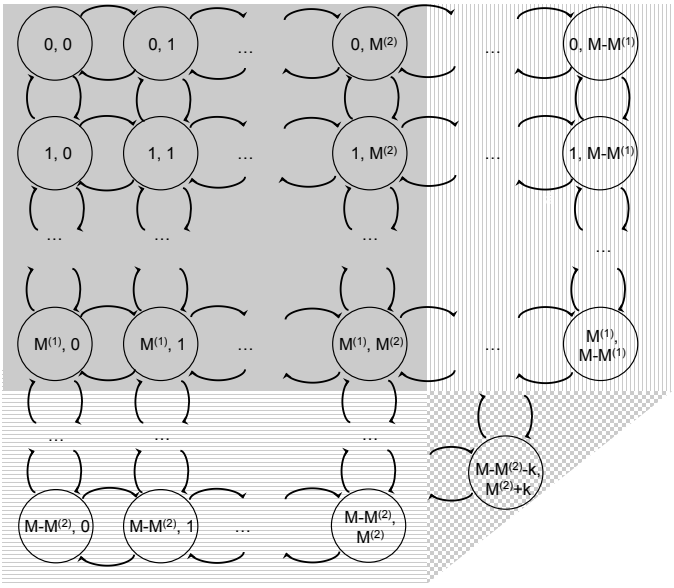

Fig. 2. CTMC describing the operation of `Network` for $S = 2$. Top-to-bottom transitions have rate $\sigma^{(1)}$, while left-to-right transitions have rate $\sigma^{(2)}$. Bottom-to-top transitions have rate $C^{(1)}$ in the first $M^{(1)}$ rows and $C^{(1)} + Q^{(1)}(a,b)$ in the remaining rows. Right-to-left transitions have rate $C^{(2)}$ in the first $M^{(2)}$ columns and $C^{(2)} + Q^{(2)}(a,b)$ otherwise.

The above service policy description resembles the operations of a multi-class processor sharing (PS) queue in which a class receives part of what cannot be used by other classes. Thus, we model the network processor of the BS with a PS queue with S classes of customers and hard limits on the number of customers in service given by $M^{(i)} + M_s$ for each class, with a global limit at M. The capacities of such classes are their dedicated capacity $C^{(i)}$ plus a portion of the shared capacity C_s. The intensities of the arrival rates are the values of the $\sigma^{(i)}$, but the shared resources are accessed only when all dedicated positions are busy.

Since the resulting queueing system, where the service rate of one class depends not only on the number of customers in that class, but also in other classes, does not admit a product-form solution (PFS) [9], we study this queue by means a continuous-time Markov chain with S-dimensional state space (one dimension per class, to count the number of services in the class) whose transitions are depicted in Fig. 2 for the case of two slices ($S = 2$), hence two customer classes. In the figure, each state of the chain reports the number of customers $m^{(1)} \leq M - M^{(2)}$ in slice 1 and $m^{(2)} \leq M - M^{(1)}$ in slice 2, subject to the constraint that $m^{(1)} + m^{(2)} \leq M$. The chain has a precise symmetry and a pentagonal shape, which is due to the above constraints.

If we denote by (a, b) the chain's state, where a is the number of services in slice 1 and b is the number in slice 2, the transition rates in Fig. 2 from state (a, b) to other states

are as follows:

$$\begin{cases} (a+1,b): & \sigma^{(1)} \ \ \forall a \le M^{(1)}-1,\ b \le M^{(2)} \\ & \quad \text{and } \forall a \le M - M^{(2)} - b - 1 \\ (a,b+1): & \sigma^{(2)} \ \ \forall b \le M^{(2)}-1,\ a \le M^{(1)} \\ & \quad \text{and } \forall b \le M - M^{(1)} - a - 1 \\ (a-1,b): & C^{(1)} \ \ \forall a \le M^{(1)} \\ (a-1,b): & C^{(1)} + Q^{(1)}(a,b) \ \ \forall M^{(1)} < a \le M - M^{(2)} \\ (a,b-1): & C^{(2)} \ \ \forall b \le M^{(2)} \\ (a,b-1): & C^{(2)} + Q^{(2)}(a,b) \ \ \forall M^{(2)} < b \le M - M^{(1)} \end{cases} \tag{25}$$

For simplicity of notation, we used the following quantities:

$$Q^{(1)}(a,b) = \begin{cases} \frac{a-M^{(1)}}{a-M^{(1)}+\max\left(0,b-M^{(2)}\right)} & \text{if } a > M^{(1)}; \\ 0 & \text{otherwise;} \end{cases} \tag{26}$$

$$Q^{(2)}(a,b) = \begin{cases} \frac{b-M^{(2)}}{b-M^{(2)}+\max\left(0,a-M^{(1)}\right)} & \text{if } b > M^{(2)}; \\ 0 & \text{otherwise.} \end{cases} \tag{27}$$

Note that different service policies (i.e., different approaches to access the shared capacity) can be accommodated in this Markov chain by just modifying transition rates.

The solution of the Markov chain can be obtained numerically with specialized tools like SMART [10]. We therefore solve the Markov chain numerically to compute $p_B^{(i)}$ as the sum of the relevant state probabilities. In the case of Fig. 2, for slice 1 we sum over states that lay on the bottom and diagonal edges, whereas for slice 2 we sum over states on the edges on the right and on the diagonal. This is because the diagonal edge at the right-bottom part of the chain in Fig. 2 contains states in which both slices suffer blocking.

The state space size of the Markov chain in Fig. 2, is $O(M^S)$, where M is the maximum number of RRC_CONNECTED terminals and S is the number of slices. Hence, being M of the order of few hundreds in real systems, the numerical solution of the Markov chain is a viable approach only for a (very) small number of slices.

G. Bounds on the performance of the `Network` *subsystem*

To mitigate the computational complexity problem, and thus be able to handle a higher number of slices, we can observe that the queuing model has, for each customer class, one queue with finite capacity constraints, Poisson arrivals, and state dependent processor service discipline. Recalling that the arrival rate at the i-th queue is equal to $\sigma^{(i)}$ and the available buffer size is equal to $M - \sum_{j=1, j\neq i}^{S} M^{(j)}$, and denoting by $\boldsymbol{m} = [m^{(1)}, m^{(2)}, \ldots, m^{(S)}]$ the S-dimensional vector of the current states of queues, and by $\mu_i(\boldsymbol{m})$ the state dependent service rate of the i-th processor sharing queue, we have that

$$\mu_i(\boldsymbol{m}) = \begin{cases} C^{(i)} & \text{if } m^{(i)} \le M^{(i)} \\ C^{(i)} + C_s \dfrac{m^{(i)} - M^{(i)}}{\sum_{j=1}^{S} \max\{0, m^{(j)} - M^{(j)}\}} & \text{otherwise.} \end{cases} \tag{28}$$

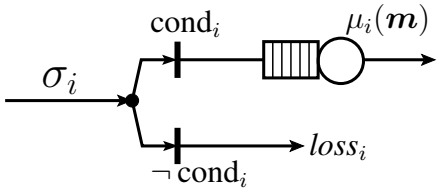

Fig. 3. Representation of the i-th queue: arrivals from `Limiter` are queued if condition (29) is satisfied, and dropped otherwise.

The previous expression for the service rate accounts for the two cases; (i) for $m^{(i)} \le M^{(i)}$ the reserved capacity $C^{(i)}$ of the i-th slice is equally shared among the $m^{(i)}$ customers; (ii) when there are $m^{(i)} > M^{(i)}$ customers, the i-th queue obtains a service rate equal to $C^{(i)}$ plus a portion of the shared capacity C_s proportional to $m^{(i)} - M^{(i)}$. Moreover, since `Network` can serve at most M customers, for all feasible states $\boldsymbol{m} = [m^{(1)}, m^{(2)}, \ldots, m^{(S)}]$ of the queueing system, we have that $\sum_{i=1}^{S} m^{(i)} \le M$ and $\sum_{j=1}^{S} \max\{0, m^{(j)} - M^{(j)}\} \le M_s$.

Arriving customers that cannot enter the i-th queue because of lack of space in the reserved positions in the queue (i.e., because they find $m^{(i)} = M^{(i)}$), or because all the shared positions are full (i.e., because they find $\sum_{j=1}^{S} \max\{0, m^{(j)} - M^{(j)}\} = M_s$) are lost.

Fig. 3 depicts the i-th queue (for $i = 1, \ldots, S$) of a queueing system with these features. The two vertical bars labeled as 'cond_i' and '$\neg\text{cond}_i$' represent the two situations that an arriving customer can encounter. In particular,

$$\text{cond}_i = \left(m^{(i)} < M^{(i)}\right) \textbf{ or } \left(\sum_{j=1}^{S} \max\{0, m^{(j)} - M^{(j)}\} < M_s\right). \tag{29}$$

If the first part of the condition does not hold, the arriving customer might be served by using the shared resources (M_s and C_s), but if the whole condition cond_i does not hold (case '$\neg\text{cond}_i$'), the arriving customer is lost, as pictorially illustrated in Fig. 3.

Several features of this model make it a non-standard multi-class queueing system (i.e., a queuing system which does not admit a PFS), where the main non-product-form characteristic concerns the rate dependency in (28). In particular, the rate of the i-th queue (for $i = 1, \ldots, S$) depends on the number of customers in all the S queues. From this follows that the derivation of the blocking probabilities requires the solution of the underlying continuous-time Markov chain (CTMC), but, as we already noted, this is feasible only for very small S (in [1] we solved the model for $S = 2$).

To avoid the complexity of a solution based on the generation of the entire state space of the `Network` model, we propose a simple modification of the model that allows to come up with a PFS queuing network. With this transformation we will be able to derive a lower and an upper bound on the blocking probabilities.

To derive the PFS bounds we modify the rate $\mu_i(\boldsymbol{m})$ of the processor sharing server for each slice $i = 1, \ldots, S$ defined in (28) by removing the dependency on the number of customers in all the other $S-1$ queues. In other words, we replace $\mu_i(\boldsymbol{m})$ with $\mu_i^{(l)}(m^{(i)})$ (resp. $\mu_i^{(u)}(m^{(i)})$) to derive a lower bound

(resp. an upper bound) on the loss probability. We derive a lower bound on the loss probability by assuming that when $m^{(i)} > M^{(i)}$ customers are in the queue, $M^{(i)}$ of them get a service rate $\frac{C^{(i)}}{M^{(i)}}$ and the remaining $m^{(i)} - M^{(i)}$ customers access shared resources with no competition from the users of other slices. Thus, we assume that `Network` allocates all shared bandwidth resources to slice i, i.e., that slice i is the only one accessing the shared bandwidth:

$$\mu_i^{(l)}(m^{(i)}) = \begin{cases} C^{(i)} & \text{if } m^{(i)} \leq M^{(i)} \\ C^{(i)} + C_s & \text{otherwise.} \end{cases} \quad (30)$$

To derive an upper bound for loss probabilities we focus our attention on the second case of (28). In particular, we can see that $M - \sum_{j=1}^{S} M^{(j)} \geq \sum_{j=1}^{S} \max\{0, m^{(j)} - M^{(j)}\}$, and hence we can write that

$$\mu_i^{(u)}(m^{(i)}) = \begin{cases} C^{(i)} & \text{if } m^{(i)} \leq M^{(i)} \\ C^{(i)} + C_s \frac{m^{(i)} - M^{(i)}}{M_s} & \text{otherwise.} \end{cases} \quad (31)$$

In this case we assume that all slices are using the shared bandwidth resources. Note that the two bounds are reached for some of the possible states of the queuing system.

By using (30), and (31) instead of (28), we can then derive lower and upper bounds for the loss probabilities (that generate, respectively, upper and lower bounds on throughput). Remarkably, the computation of the bounds can be done by exploiting their PFS. Indeed, to compute the measures we are interested in, we can use the efficient normalization constant computation algorithm proposed in [11][2] whose computational complexity is $O(S \cdot M^2)$, where M is the maximum number of users in the RRC_CONNECTED state and S is the number of slices.

Note that the bounds are not directly applicable to different service disciplines (i.e., different algorithms for accessing the shared BS capacity), but approaches similar to the one just described can be devised also for other cases.

The main question of any bounding technique concerns the tightness of the provided bounds. To answer this question we will show various numerical examples in the performance evaluation section. Here we remark the fact that the bounds are different only if the slices can use shared resources, and the distance between lower and upper bounds depends on the quantity of shared capacity and positions in the `Network` subsystem. However, for all those cases in which the `RACH` subsystem constitutes the main performance bottleneck, shared resources at `Network` remain unused, so that the bounds (practically) coincide and yield the exact solution.

H. Access Time Distributions

The cumulative distribution of the time $T^{(i)}$ spent in one access attempt in slice i is the one resulting from the following events that partition the space of probabilities: timeout, success or network blocking in stage k, and excess RACH retries. In case of timeout, the time spent is $T_O^{(i)}$. In case of success or network blocking in stage k, the time spent in the access attempt is the r.v. $Y_{k-1}^{(i)} + Z$, conditional to the event that the timeout does not expire. In case of excess RACH retries, the time is $T_{\max}$ (for the last retry with no BS answer) plus the r.v. $Y_{k_{\max}-1}^{(i)}$ (which accounts for previous retries), conditional to the event that the time at the end of the last but one attempt allows for an extra $T_{\max}$ in the last attempt. The result is as follows:

$$\begin{aligned} F_{T^{(i)}}(x) = {} & P_{TO}^{(i)} \, \mathcal{U}\left(x - T_O^{(i)}\right) \\ & + \sum_{k=1}^{k_{\max}^{(i)}} \frac{F_{Y_{k-1}^{(i)}+Z}(x)}{F_{Y_{k-1}^{(i)}+Z}\left(T_O^{(i)}\right)} \left(P_S^{(i)}(k) + P_B^{(i)}(k)\right) \\ & + P_N^{(i)}\left(k_{\max}^{(i)} + 1\right) \frac{F_{Y_{k_{\max}^{(i)}-1}^{(i)}}(x - T_{\max})}{F_{Y_{k_{\max}^{(i)}-1}^{(i)}}\left(T_O^{(i)} - T_{\max}\right)}, \end{aligned} \quad (32)$$

where $\mathcal{U}\left(x - T_O^{(i)}\right)$ is a unit step at time $T_O^{(i)}$. As a corollary of (32), note that the CDF of the time spent for one service request in case of success is

$$F_{T^{(i)}}(x|\text{Success}) = \frac{1}{P_S^{(i)}} \sum_{k=1}^{k_{\max}^{(i)}} \frac{F_{Y_{k-1}^{(i)}+Z}(x)}{F_{Y_{k-1}^{(i)}+Z}\left(T_O^{(i)}\right)} P_S^{(i)}(k). \quad (33)$$

IV. Numerical Results

In this section we study a few cases of sliced BS resources, which correspond to realistic application scenarios. In all cases we consider a BS with user plane capacity equal to 100 Mb/s that must transmit messages of HTC type with average length 1.2 Mb, and with average length 8 kb in case of MTC; the number of RACH preambles is equal to 54, and the number of positions in the RRC_CONNECT state is 200.

In Table II we provide, for four instances of a BS with two slices, one carrying MTC traffic and one HTC, the shares of traffic (referred to the intensity of access requests, population (referred to the number of devices) and BS capacity dedicated to the two slices. The table also reports the number of dedicated RACH preambles and positions in the RRC_CONNECTED state, and the timeout values. The resources which are not dedicated to slices can be evenly shared. Later we will also address the case of coexistence of larger numbers of slices, considering examples with three and six slices, respectively. The two-slice scenarios that we consider are as follows:

- **Sparse IoT** – A BS serving a urban cell with mostly HTC traffic, and a small slice for IoT (MTC) traffic.
- **Dense IoT** – A BS serving a cell with mostly MTC access requests characterized by low traffic, so that a large part of the capacity is used by a slice with few HTC devices.
- **Small Factory** – A BS serving a urban area with mostly HTC traffic, but devoting a slice to serve a urban industrial settlement, with MTC traffic.
- **Big Factory** – A BS serving a private area (such as a smart factory) with mostly MTC traffic, and a slice to handle HTC traffic.

[2]That paper presents a computational efficient algorithm for a class of product-form models that represent a generalization of the PFS queuing networks with population size constraints.

TABLE II
SLICE PARAMETERS FOR THE CONSIDERED APPLICATION SCENARIOS WITH TWO SLICES (COLUMNS LABELED AS 'H' REFER TO HTC DEDICATED RESOURCES, 'M' IS USED FOR MTC AND 'S' FOR SHARED RESOURCES)

Scenario	Access request share		Population share		Capacity [Mb/s]			Preambles			Positions			Timeout [s]	
	H	M	H	M	H	M	S	H	M	S	H	M	S	H	M
Sparse IoT	0.95	0.05	0.79	0.21	80	2	18	40	5	9	100	10	90	5	5
Dense IoT	0.05	0.95	0.05	0.95	75	5	20	10	40	4	40	100	60	3	1
Small factory	0.75	0.25	0.97	0.03	50	20	30	30	10	14	50	50	100	5	0.1
Big factory	0.3	0.7	0.81	0.19	10	50	40	10	30	14	20	150	30	5	0.1

In the numerical evaluation, we assume that HTC devices on average, considering video, voice and data applications, generate one message per second—i.e., each device offers a traffic of 1.2 Mb/s—while for MTC devices the timeout corresponds to the message generation interval, so to emulate the process of updating the status of a system. This corresponds to generating 8 to 80 kb/s per MTC device in the settings of Table II, but we will also explore more extreme cases, generating 0.8 to 800 kb/s per MTC device. Table II reports, for each slice and each scenario, both the share of access requests and the corresponding share of population of devices, computed according to the message generation rate of each HTC or MTC device.

A. Validation

In order to validate the analytical model, we used an ad hoc simulator written in C++. This is an event-based simulator that represents with high accuracy the standard operations necessary to register the terminal at the BS, and to access and use the BS resources. The fact that the simulator closely follows the standard 3GPP procedures allows us to validate the simplifying assumptions introduced in the analytical model for the sake of tractability.

Fig. 4 compares analytical and simulation results, with their 95% confidence intervals. Notwithstanding the approximations introduced in the model, the figure shows a very good match between model and simulation, up to very high offered loads (more than 7 Gb/s as shown in the x-axis of the figure), which corresponds to large device populations (up to a few tens of thousands of devices, as shown in the secondary x-axis, which maps the offered load onto the number of devices).

B. Throughput

Figs. 4 to 7 illustrate the behavior of the system throughput (at `RACH`, `Decoder` and `Network`) for the four considered two-slice scenarios. In the Sparse IoT case, HTC saturates first, and the HTC load on `RACH` has only a minor impact on the traffic of MTC. This indicates that light MTC traffic with non-stringent delay requirements is not hard to accommodate. The Dense IoT case is more interesting. It shows that the MTC and HTC saturation regions superpose. Here, the activity of MTC in `RACH` heavily affects HTC performance. Therefore, supporting the coexistence of HTC and MTC slices in such scenarios is challenging. If we go back to the Small Factory case used above for validation, we notice only minor differences with the Sparse IoT case. However, in this case, the limited resources allocated to HTC make it easier to avoid impairments for MTC. More critical is the Big Factory case, in which the MTC traffic is predominant and yet a small amount of HTC connections can seriously hinder MTC performance at relatively low aggregate traffic rates, while under heavy traffic the impact of HTC on the throughput of MTC is less relevant.

The figures also show that the losses due to `Decoder` are negligible for MTC, while they have to be taken into account for HTC. This is due to the fact that we have set a power ramping offset for MTC ($o^{(1)} = 2$), while HTC does not use any offset. This tells of the importance of the power ramping offset in the slice configuration.

Due to the heterogeneity of slices, there are no clear optimal device population sizes at which all slices receive the maximal throughput. In all cases, the HTC slice works better with a few hundreds of devices, while MTC achieves the highest `Network` throughput with a few thousands of devices. Considering the Dense IoT scenario, which shows the highest density of MTC devices (95% of the total), our study shows that a cell can sustain about 2000 MTC devices. If we consider instead the Small Factory case, with the highest density of HTC devices (97%), we can observe that the `Network` subsystem of a cell saturates with as few as 300 HTC devices.

C. Access Delay

The numerical results of access delay (the time elapsing from the request generation until the start of the message transmission) for MTC and HTC traffic are shown in Figs. 8 and 9, respectively. Note that in this case we use service requests per second as the horizontal axis metric; this is necessary because the throughput per access request is different in the four two-slice scenarios that we compare: in Sparse IoT each access request corresponds on average to 1.14 Mb, in Dense IoT to 67.6 kb, in Small Factory to 902 kb, and in Big Factory to 365.6 kb. In the case of MTC, the two curves for Small Factory and Big Factory saturate at 100 ms, which is the timeout for those cases. The other two cases remain well below their timeout values which are much less stringent. In the case of HTC, we see that all curves saturate at the same value, which is close to 2.25 s, due to the maximum permitted number of retries, and the average backoff delay equal to 0.25 s. To this we must add $10 \cdot T_{\max}$, which is however just about 0.13 s. The Small Factory scenario saturates first because a large fraction of the BS traffic is associated with only a small portion of dedicated resources. The Dense IoT scenario yields

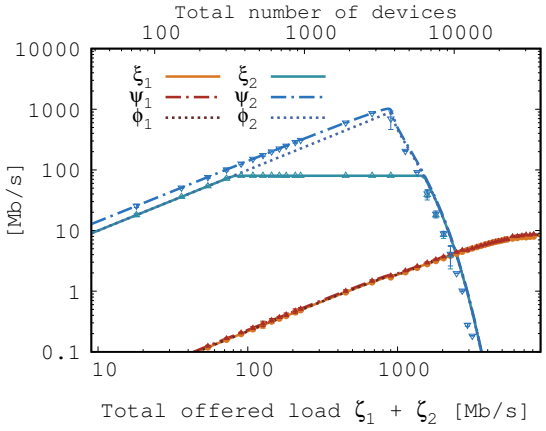

Fig. 4. Small Factory throughput (in Mb/s) at RACH (Ψ), Decoder (ϕ) and Network (ξ) vs. offered load (in Mb/s and in number of devices); lines represent the model, markers with confidence intervals are for simulations; HTC in blue, MTC in red.

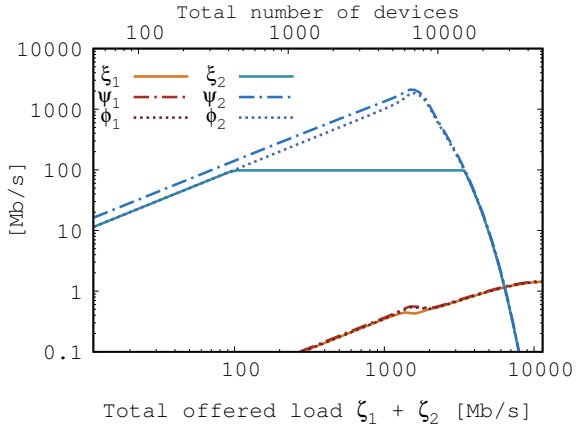

Fig. 5. Sparse IoT throughput (in Mb/s) at RACH (Ψ), Decoder (ϕ) and Network (ξ) vs. offered load (in Mb/s and in number of devices); HTC in blue, MTC in red.

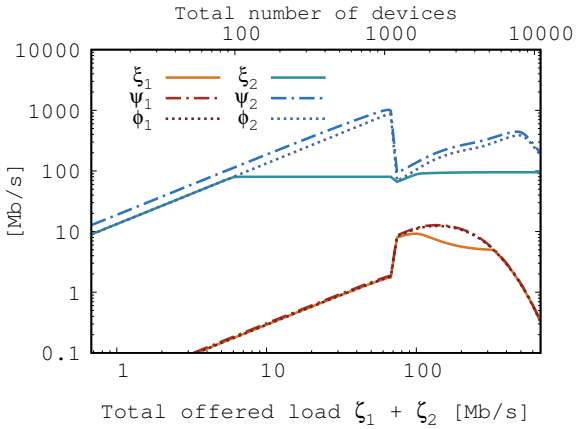

Fig. 6. Dense IoT throughput (in Mb/s) at RACH (Ψ), Decoder (ϕ) and Network (ξ) vs. offered load (in Mb/s and in number of devices); HTC in blue, MTC in red.

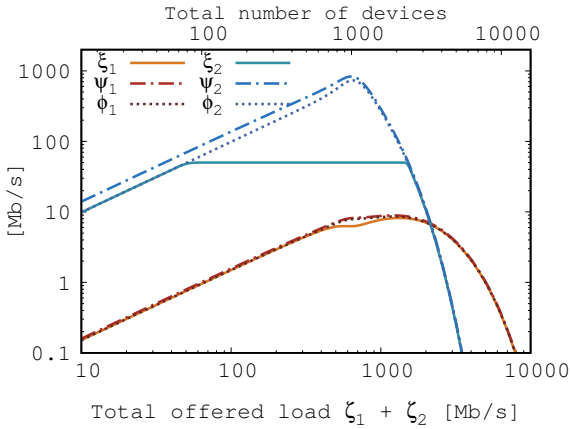

Fig. 7. Big factory throughput (in Mb/s) at RACH (Ψ), Decoder (ϕ) and Network (ξ) vs. offered load (in Mb/s and in number of devices); HTC in blue, MTC in red.

the lowest delays because its traffic share is very low, and the reserved resources prove to be sufficient to achieve low delay.

D. Success Probability

Success probabilities for the four considered scenarios are presented in Figs. 10 and 11 for MTC and HTC traffic, respectively. In the MTC case, Small Factory and Big Factory suffer from the very low timeout values, but achieve good success probabilities up to about 1000 requests/s. Beyond this value, the RACH subsystem approaches saturation, and retrials make timeouts more likely. In the case of HTC, we see very high success rates in the Dense IoT scenario, due to the fact that the HTC traffic share in this case is very low, and resources reserved to HTC are largely sufficient.

E. Lesson Learnt from the Two-slice Scenarios

One of our key observations is that the saturation of RACH is a critical issue, and unexpected behaviors are observed for the traffic loads that bring the RACH to saturation. In Fig. 12 we plot the probability of reaching the timeout for MTC traffic versus the HTC traffic load in the Big Factory scenario, assuming that the MTC traffic is fixed at 8 Mb/s, and that the number of preambles reserved for MTC is varied between 20 and 40. We clearly see a bump in the timeout probability that corresponds to HTC traffic values that lead to RACH saturation. After this point, HTC consumes little Network resources, but saturates the RACH, so that there is a clear need to protect MTC by allocating a large number of dedicated preambles. If the number of dedicated preambles is too small, the timeout probability settles at unacceptable values.

Moreover, considering throughput and delay figures, with the parameters used in the discussed experiments—which are typical of networks slowly evolving towards 5G—we can expect to sustain populations of at most a few hundreds of HTC devices or a few thousands of MTC devices. Of course, as we can see from Figs. 10 and 11, approaching such limit numbers implies lower success probabilities. This gives rise to a tradeoff for the network operator, that can exploit accurate modeling techniques, like the one we propose in this paper, to select the operational point for the network.

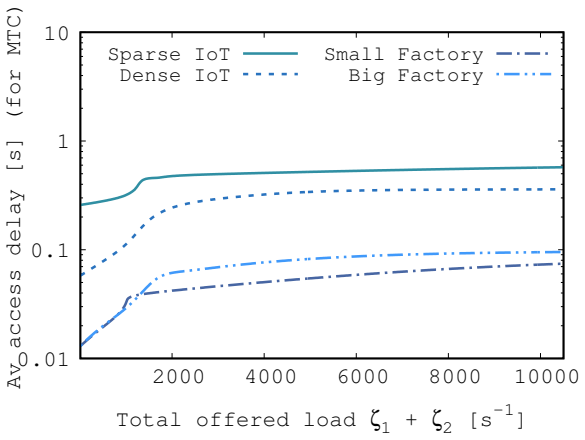

Fig. 8. Average access delays for slice 1 (MTC) in seconds for the four different scenarios versus the total load offered to the BS in service requests per second

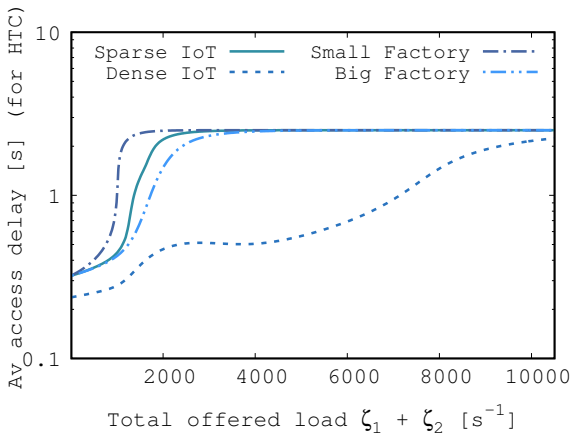

Fig. 9. Average access delays for slice 2 (HTC) in seconds for the four different scenarios versus the total load offered to the BS in service requests per second

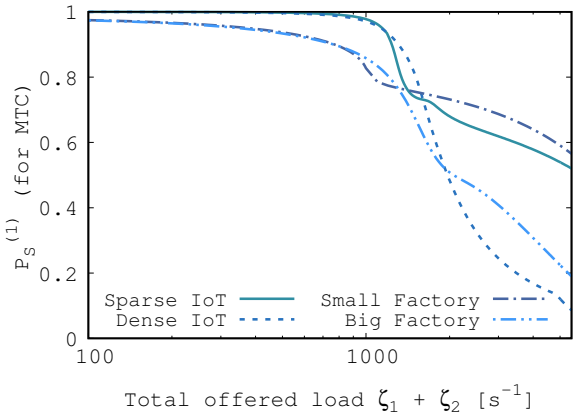

Fig. 10. Success probability for MTC for the four different scenarios versus the total load offered to the BS in service requests per second

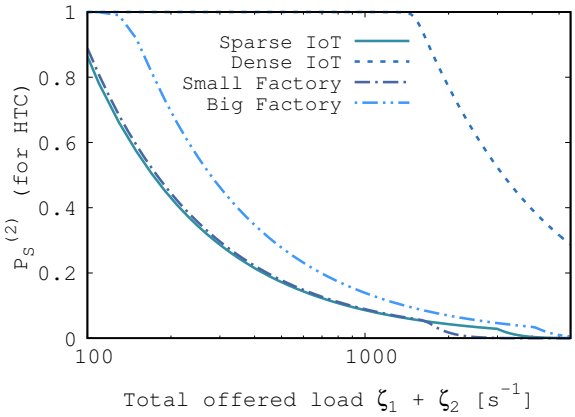

Fig. 11. Success probability for HTC for the four different scenarios versus the total load offered to the BS in service requests per second

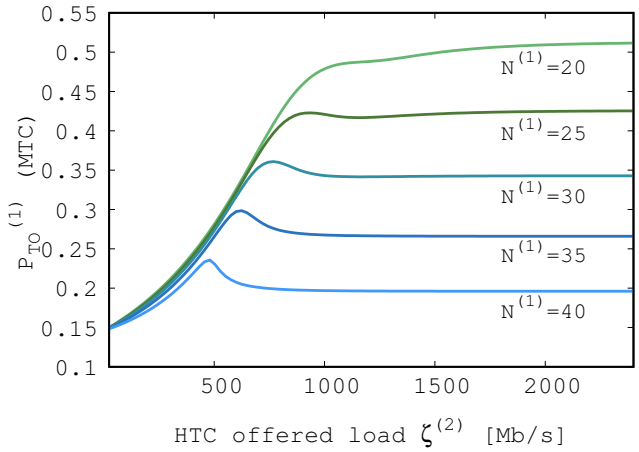

Fig. 12. Timeout probability for MTC at fixed MTC service request rate $\zeta^{(1)} = 8$ Mb/s versus the load offered by HTC in Mb/s

F. Increasing the Number of Slices

We now analyze more complex scenarios, involving the coexistence of more than two slices. Since the complexity of the corresponding CTMC describing the Network subsystem scales exponentially, we use these examples to validate the alternative approach proposed in Section III-G, which is based on the use of smart, non-trivial bounds. We performed an extensive set of numerical experiments to compare the performance measures obtained with the bounding technique against those that can be derived by using (when feasible) the CTMC approach.

1) A first three-slice scenario: We first consider a scenario with light MTC traffic and two highly loaded HTC slices. The scenario could represent a cell with two tenants for public data access plus an IoT operator, with the realistic parameter set shown in Table III.

Note that, since it can be expected that the bounds are extremely tight when the fraction of shared resources is small, we leave unassigned 30% of capacity and two thirds of Network positions. Like for previous experiments with two slices, the BS capacity is set to 100 Mb/s, HTC service requests correspond to 1.2 Mb messages on average, and MTC traffic corresponds to small messages of 8000 bits. In this case, the offered load fractions for the three slices are 0.6 and 0.3 for HTC slices, and 0.1 for the MTC slice (this corresponds to having 99% of devices on the HTC slices). The reserved capacities for the three slices are respectively 40, 20 and 10

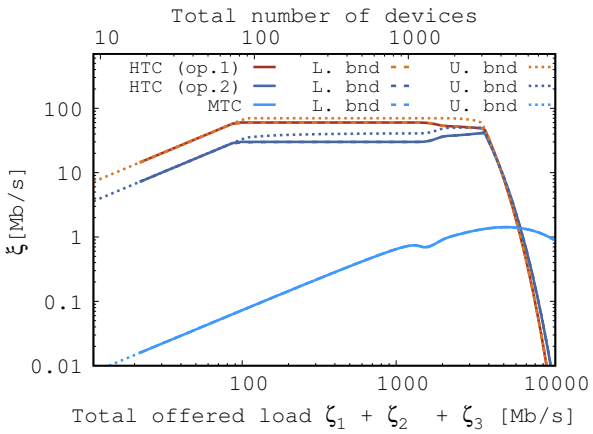

Fig. 13. Exact Network throughput values and bounds for the three-slice scenario of Table III vs. the total load (in Mb/s). The secondary x-axis reports the total number of devices resulting from the composition of the three slices.

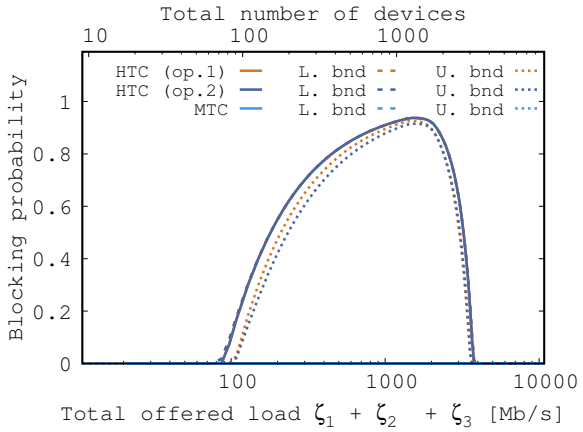

Fig. 14. Exact values and bounds for blocking probability in the three-slice scenario of Table III (MTC slices incur no blocking) vs. the total load (in Mb/s). The secondary x-axis shows the total number of devices resulting from the composition of the three slices.

TABLE III
CONFIGURATION FOR THE CASE OF THREE SLICES WITH HIGHLY LOADED HTC SLICES AND LIGHT MTC TRAFFIC

Slice	Access request share	Population share	Capacity [Mb/s]	Preambles	Positions	Timeout [s]	Duty Cycle [s]
HTC (operator 1)	0.6	0.66	40	30	40	5	1
HTC (operator 2)	0.3	0.33	20	15	20	5	1
MTC (IoT)	0.1	0.01	10	5	5	0.1	0.1
Shared	N/A	N/A	30	4	135	N/A	N/A

Mb/s, so that 30 Mb/s are shared. Note that the share of traffic offered by MTC is less than the share of capacity reserved to MTC at the Network, so MTC is not expected to use much of shared capacity unless all slices are overloaded. Out of the 54 available RACH preambles, 30 plus 15 are allocated to HTC slices, and 5 to the MTC slice. Of the 200 positions in the RRC_CONNECTED state, 40 and 20 respectively are allocated to the two HTC slices, and 5 to the MTC slice, so that 135 positions are shared. The timeouts for the access requests of the two HTC slices are equal to 5 s, while the timeout for the MTC slice is 0.1 s.

The curves in Fig. 13 plot the throughput—in terms of exact values and bounds, expressed in Mb/s—of the three slices as a function of the total offered load and, in the secondary x-axis, the total number of devices. The two HTC slices saturate their available capacity, as shown by the flat part of the curves, while the MTC slice, because of its much smaller message size and its dedicated resources, does not reach saturation. Since we have a net predominance of HTC devices, the population that can be efficiently sustained includes at most about one hundred devices.

The bounds are indistinguishable from the exact solution in the case of the MTC slice, as well as for the two HTC slices before saturation. The bounds can be seen to be tight also for the two HTC slices when in saturation, where the exact solution almost overlaps with the lower bound. This is because the two slices saturate at the same offered load value, so that the condition in (31) is satisfied with high probability. The upper bound is not far either, at least in this case in which the MTC does not practically use shared resources, while the two HTC slices contend for shared resources. Fig. 14 shows that blocking probability bounds are very tight for the HTC slice with higher throughput, while they are slacker for the other HTC slice. Note that the lower bound for throughput is an upper bound for the blocking probability and vice versa (for consistency, the terms 'lower' and 'upper' used in the labels of the figures refer to throughput bounds). The only region in which bounds can be large is a small interval around the first knee of the throughput curve, where the blocking probability is however low.

2) A second three-slice scenario: We now consider a different three-slice scenario, one in which HTC and MTC traffic are comparable, no slice receives enough dedicated resources to serve all its traffic as it grows, and in which shared resources are abundant (i.e., 95% of capacity and 50% of positions are shared). Specifically, we consider one slice for HTC and two for MTC, with the parameters described in Table IV. Here the number of MTC devices is not negligible, as it accounts for about 9% of the population. The scenario could represent the case of an industrial site with a public data service on HTC and two MTC slices for two separate factories. We assume half of access requests are for HTC and the other half is equally split across the two MTC slices, although one MTC slice receives more resources than the other. Most of the capacity is left in the shared pool, because we have assumed that the HTC slice does not need stringent guarantees and the MTC devices need little capacity. The scenario was deliberately chosen with a large amount of shared capacity, so

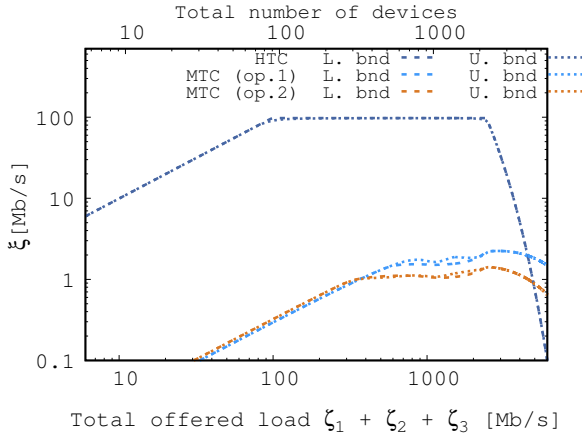

Fig. 15. Network throughput bounds for the three-slice scenario of Table IV with 2.5, 1.5, and 1 Mb/s of capacity assigned to the three slices (i.e., 95 Mb/s of shared capacity) versus the total load in Mb/s (lower x-axis) and total number of users (upper x-axis)

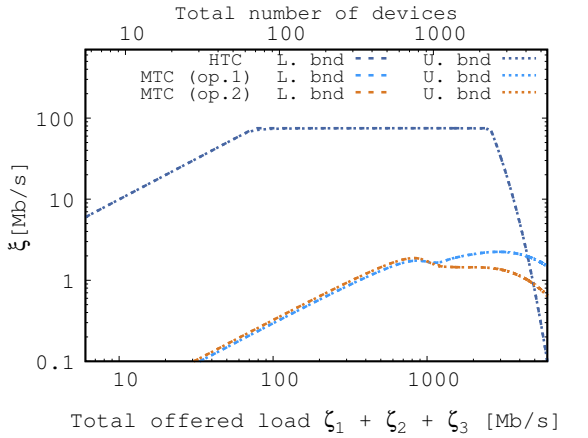

Fig. 17. Network throughput bounds for the three-slice scenario of Table IV with 25, 15, and 10 Mb/s of capacity assigned to the three slices (i.e., 50 Mb/s of shared capacity) versus the total load in Mb/s (lower x-axis) and total number of users (upper x-axis)

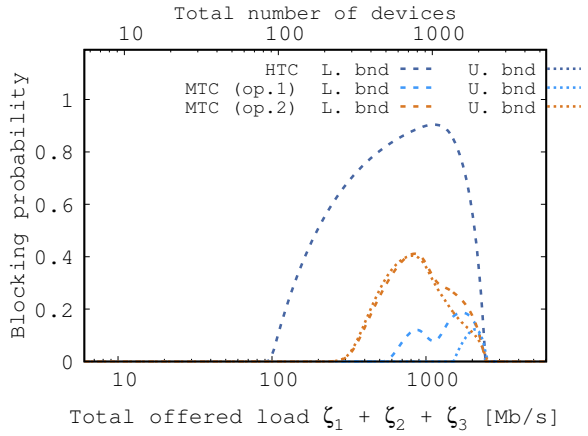

Fig. 16. Blocking probability bounds for the three-slice scenario of Table IV with 2.5, 1.5, and 1 Mb/s of capacity assigned to the three slices (i.e., 95 Mb/s of shared capacity) versus the total load in Mb/s (lower x-axis) and total number of users (upper x-axis); MTC incurs no blocking

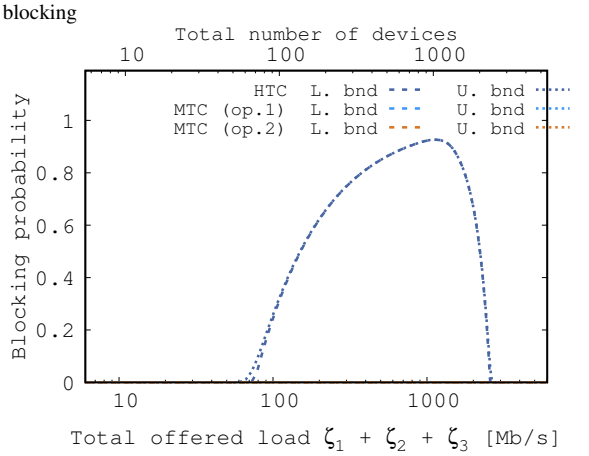

Fig. 18. Blocking probability bounds for the three-slice scenario of Table IV with 25, 15, and 10 Mb/s of capacity assigned to the three slices (i.e., 50 Mb/s of shared capacity) versus the total load in Mb/s (lower x-axis) and total number of users (upper x-axis); MTC incurs no blocking

as to stress the differences between bounds in the computation of the throughput of Network (cf. the impact of C_s on the bounds (30)–(31)).

Notwithstanding the large amount of shared resources, Fig. 15 shows that, for this case, the two bounds are very close. Limited differences can be noted for the HTC slice, in the region of saturation of Network. Similarly, the bounds calculated on the blocking probability, shown in Fig. 16, are quite tight for HTC and the MTC with less reserved resources, while being looser for the other MTC slice. This behavior is due to the aggressive access to shared resources by HTC only, which makes shared resources highly utilized. In contrast, MTC slices do not overload the Network subsystem even when they have little dedicated resources. However, shared positions are used by all slices. Note in fact that when the HTC RACH throughput reaches its peak for the HTC slice (not shown in the figure, it can be however intuitively identified at around 1 Gb/s from the shape of the throughput before and after the flat zone imposed by the Network), the pressure of HTC diminishes, and MTC slices obtain more resources. Although they do not saturate the Network subsystem throughput, still this behavior indicates that MTC devices use more shared positions, which are the ones freed by HTC after the RACH subsystem cuts off. The total population that can be served in this mixed slice case with little dedicated resources is quite low, of the order of 200 devices (about 180 for HTC and 20 for MTC) before the Network throughput saturates for all slices. This means that a large pool of shared resources has negative impact on the size of the sustainable population.

If we now increase the amount of bandwidth allocated to slices to 25, 15 and 10 Mb/s for the HTC, MTC (operator 1) and MTC (operator 2) slices, respectively, we obtain the results shown in Figs. 17 and 18. We can see that, as expected, by reducing the amount of shared resources the bounds have become even tighter than before. In addition, we can observe an improvement in the performance of the two MTC slices, both in throughput and loss probability, which is natural, since we have increased the amount of resources for their exclusive use.

TABLE IV
CONFIGURATION FOR THE CASE OF THREE SLICES WITH HIGH MTC TRAFFIC AND ABUNDANT DEDICATED RESOURCES

Slice	Access request share	Population share	Capacity [Mb/s]	Preambles	Positions	Timeout [s]	Duty Cycle [s]
HTC (public)	0.5	$0.\overline{90}$	from 2.5 to 49.5	25	50	5	1
MTC (operator 1)	0.25	$0.0\overline{45}$	from 1.5 to 29.7	10	30	0.1	0.1
MTC (operator 2)	0.25	$0.0\overline{45}$	from 1 to 19.8	5	20	0.1	0.1
Shared	N/A	N/A	from 95 to 1	14	100	N/A	N/A

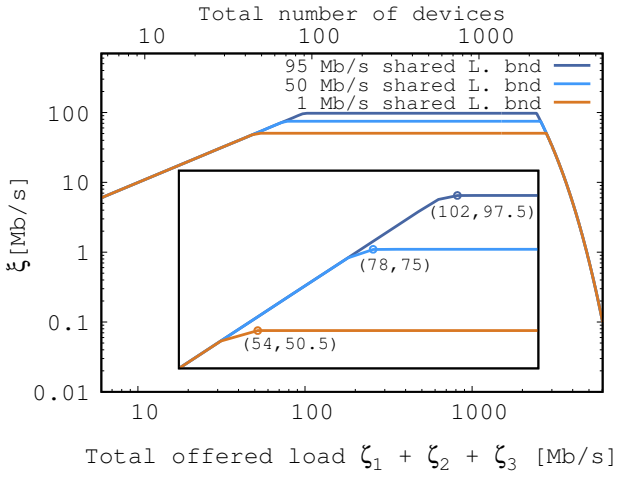

Fig. 19. `Network` throughput lower bounds (upper bounds are undistinguishable) for the HTC slice in the three-slice scenario of Table IV with different amounts of shared capacity (i.e., 95, 50, and 1 Mb/s) versus the total load in Mb/s (lower x-axis) and total number of users (upper x-axis). The inset shows the portion of the curves where the network throughput saturates

In particular, no loss is now observed for MTC traffic. This comes at the cost of a slight reduction in the performance of HTC traffic, in terms of both saturation throughput and number of users. This reduction is better appreciated in Fig. 19, where we show the throughput of the HTC slice with 95, 50 and 1 Mb/s of shared capacity (while the rest of parameters remain unchanged, see Table IV). We clearly see that a reduction of the shared capacity penalizes the HTC slice, whose saturation throughput decreases from 97.5 to 75 and to 50.5 Mb/s. In the first case the decrease brings a benefit to the two MTC slices, at least in terms of loss probability. Instead, the second decrease does not impact the MTC slices performance. This implies that in the case of several competing slices, the choice of the amount of resources to allocate to individual slices, and consequently of the amount of resources shared among them, is a critical management issue. Too many statically allocated resources imply less flexibility, and penalize the high traffic slices. On the other hand, too many shared resources penalize the low traffic slices, because the high traffic slices tend to grab most of the shared bandwidth. A careful balance is necessary, which depends on the specific slice configuration, and requires simple but accurate models, like the one we presented in this paper, to predict the performance outcome of the resource partitioning.

3) A six-slice scenario: So far, we have observed a very good accuracy of our proposed bounds in many tested configurations. This allows us to conclude that the bounds offer a good approximation for the case of three slices. However, this does not exclude a different behavior for a higher number of slices. Thus, in order to show the ability of our approach to cope with more challenging cases, Fig. 20 shows the throughout for a case with six slices, with the configuration shown in Table V, and with the data volume of requests associated to HTC and MTC traffic specified for the previously described experiments.

This scenario could represent the case of a cell covering a city hospital and its neighborhood. Here we selected two HTC slices (e.g., one for public access and one reserved to the personnel of the hospital) plus four MTC slices (e.g., one for a factory, one for generic IoT, one for coordinating vehicles in the neighborhood, and one for hospital devices). The slices are very heterogeneous and they are assigned realistic amounts of dedicated resources, in a very heterogeneous way. Shared resources are limited in terms of capacity, while they are more generous in terms of RACH preambles and service positions in `Network`. Here, one HTC slice saturates before the other because of the different number of reserved RACH preambles, being the rest of parameters for HTC slices the same. MTC slices are basically of two kinds. Three of the four MTC slices are access-intensive and have large portions of capacity, preambles and positions reserved for their exclusive use. They behave similarly, although experiencing a different cutoff, due to different numbers of dedicated positions. However, one more MTC slice has very little traffic and no dedicated resources. For this slice, we observe saturation effects at `Network`. Although here the MTC population covers about 20% of the total, most of the BS resources are dedicated, which allows to serve up to 500 devices before the MTC slice without dedicated resources collapses.

As in the cases with three slices, here we observe non-coincident bounds only in the regions in which slices saturate on `Network`. In all cases, bounds are close enough to provide decent approximations. Similarly, Fig. 21 shows close bounds for the blocking probability of HTC slices and for the MTC slice with no dedicated resources (other slices incur no blocking)

Note that bounds are very important because, although on the one hand they introduce some approximation, on the other hand they allow the analysis to scale to otherwise unfeasible cases. For instance, with the above-discussed six-slice configuration, it took less than an hour to compute the 590 points per bound per slice (about 7k points in total) that compose Fig. 20, while it took more than a week to solve the CTMC for the much simpler case with three slices, and it was not conceivable to use the CTMC for the case of six slices

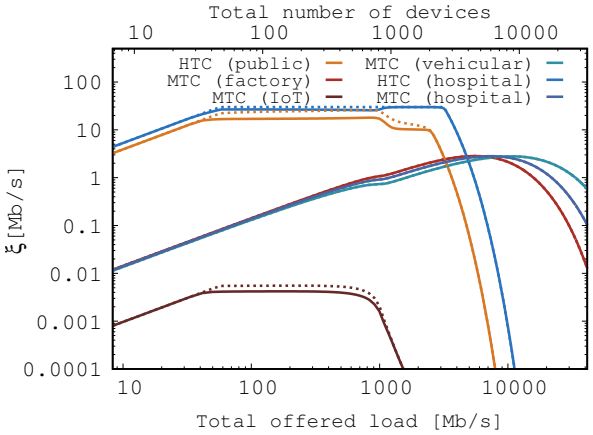

Fig. 20. Network throughput bounds for the six-slice scenario of Table V (Solid lines for lower bounds - dashed lines for upper bounds) vs. the total load (in Mb/s, lower x-axis) and total number of users (upper x-axis)

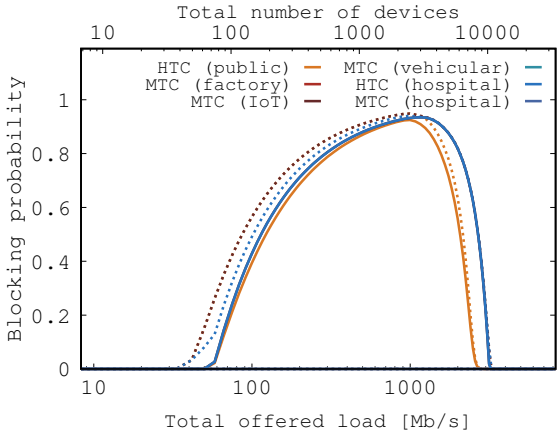

Fig. 21. Blocking probability bounds for the six-slice scenario of Table V (Solid lines for upper bounds - dashed lines for lower bounds) vs. the total load (in Mb/s, lower x-axis) and total number of users (upper x-axis)

TABLE V
CONFIGURATION PARAMETERS FOR THE CASE OF SIX SLICES

Slice	Access request share	Population share	Capacity [Mb/s]	Preambles	Positions	Timeout [s]	Duty Cycle [s]
HTC (public)	0.27	0.3985	10	5	10	5	1
MTC (factory)	0.15	0.0221	20	10	20	0.1	0.1
MTC (IoT)	0.01	0.1476	0	0	0	10	10
MTC (vehicular)	0.15	0.0221	20	10	30	0.01	0.01
HTC (hospital)	0.27	0.3985	10	10	10	5	1
MTC (hospital)	0.15	0.0111	20	10	40	0.05	0.05
Shared	N/A	N/A	20	8	90	N/A	N/A

with a machine equipped with an Intel Xeon CPU E5-1620 v3 @ 3.50GHz.

Besides good accuracy of the bounds, the figures for scenarios with multiple slices show that the interaction between slices becomes evident only when one or more slices, but not all of them, experience a bottleneck in Network *and* the RACH drops requests aggressively. This has negative impact on the affected slices but also frees resources for other slices (see, e.g., the changes of slope for the throughput with more than 2 Gb/s in Fig. 15 and for more than 1 Gb/s in Fig. 20). Most importantly, some slices can incur RACH or Network bottlenecks well before other slices, so that it is not easy to correctly dimension the resources to be allocated to each slice. However, our model, with the bounding technique we propose, offers a powerful tool to identify and test suitable configurations with limited computational complexity.

V. RELATED WORK

An overview of network slicing concepts, architectures and algorithms was recently provided by two special issues of the IEEE Communications Magazine [12], [13]. Moreover, network slicing in the RAN and heterogeneous traffic types are being investigated under different perspectives, although not yet from the point of view of their compound requirements and interactions.

Resource allocation is one of the key challenges to tackle, and, accordingly, a number of proposals are sprouting these days. For instance, the authors of [14] propose an orchestration system that leverages deep learning techniques, so as to follow traffic fluctuations and allocate resources to slices accordingly. A study of the dynamic allocation of base station resources to network slices is considered in [15]. The selected resource sharing model is a Fisher Market in economics terms. It is shown to provide each slice with the same or better utility than a static resource allocation and to admit a Nash equilibrium. The performance of the proposed approach is again investigated by simulation. More practical studies like [16] show via simulation that earliest deadline first (EDF) scheduling represents a practical and effective solution for performance isolation with dynamic resource allocation in RAN slicing scenarios. The optimal allocation of resources to slices is addressed in [17], where a distributed algorithm is proposed and analyzed by simulation, considering a dense small cell deployment, and showing that substantial capacity savings can be achieved while providing a given QoS to end users. Furthermore, the authors of [18] show that physical transmission resources can be sliced using millimeter wave techniques, while the authors of [19] demonstrate that physical resources assigned to slices need to be coordinated across multiple cells, otherwise slices cannot fully exploit the properties of physical level protocols. Other studies show the importance of per-slice resource allocation to satisfy non-trivial performance indicators [20]. There are also active initiatives devoted to develop concepts and implementations of network slicing, e.g., the European Commission-founded projects 5G-CROSSHAUL [21], 5G-TRANSFORMER [22], and 5G-NORMA [23]. However,

the existing approaches somehow neglect the role of network access procedures, which, as we have shown in this article, can introduce unexpected behavioral trends in the access network.

Besides resource allocation, there are several works pointing at performance issues of network slicing, and proposing optimization schemes. E.g., in [24], a dynamic RAN cell slicing controller was proposed and evaluated by simulation in a urban setting comprising 19 microcells, showing that the proposed controller performs better than a distributed static slicing solution and a centralized load balancing solution. The authors of [25] further present radio slicing implementation with 5G NR and discuss potential slice configurations, while the use of machine learning to manage the resources of 5G radio slices is discussed in [26]. An optimization problem for radio resource sharing among slices in a cell is studied in [27], that also proposes an efficient algorithm for optimization. Simulation results show good isolation and an increase in the multiplexing gain by sharing unused resources. The joint optimization of admission control, user association, baseband and radio resource allocation is proposed in [28]. Simulation results show that the proposed scheme achieves better performance than baseline schemes. The authors of [29] propose to use a Cross Layer Controller to orchestrate SDN and SDR technologies, so to unify the control of radio and transport protocols; they use simulations to show that significant gain stems from the coordination of slicing in different network segments. The analysis of the market composed by one infrastructure provider and several tenants that rent a network slice to provide service to their customers is tackled in [30]. A slice admission control algorithm is designed to maximize the revenues of the infrastructure provider while providing the expected performance to the slice users. The performance of the proposed algorithm is evaluated by simulation. The sharing of resources among slices is investigated in [31]. Each slice is assigned a fixed portion of available resources, which are then equally distributed to slice users. Newly arriving users are accepted by slices with autonomous decisions based on a game that admits a Nash equilibrium. The effectiveness of the proposed solution is studied by simulation. The introduction of a limit on the number of resource blocks allocated to each slice in a base station (BS) to guarantee resource isolation is proposed in [32]. The authors show that this approach combined with slight modifications of the ordinary packet scheduling algorithm can provide the desired isolation. In some cases an improvement in throughput with respect to a static bandwidth partitioning is observed in simulation results. This body of work is important, although we claim that the techniques proposed in there should be revisited to take in consideration the presence of potential RACH bottlenecks. Our model could be used to enable such study.

More specifically, our work is different from the previous literature because we consider for the first time network slicing together with the details of the algorithms that rule the operations on the radio interface of a base station. In addition, our analysis is based on a detailed analytical model of the base station operations, which allow for the derivation of exact—through computationally complex—expressions for the key performance indicators, given a slice-set configuration. They also allow to derive non-trivial tight bounds for blocking probability and throughput, which scale efficiently in the analysis of several slices. Note that, in our case, simulation just serves the purpose of validating the accuracy of the analytical model. Note also that our results are not meant to contrast the findings of other works, neither they are proposing novel resource management methods. Instead, our model and bounds shed light on the intricacies of RAN sharing mechanisms in an interpretable manner, and are instrumental in enhancing and speeding up resource management optimization tools like the ones mentioned in this section.

VI. Conclusions

In this paper we described a detailed stochastic model of the behavior of radio access in a sliced RAN cell, including most features of the standard access procedures. Our model allows the investigation of the effect of the allocation of resources to slices on the radio interface of one cell, hence the correct setting of the slice parameters.

Looking at the case of one typical cell comprising one HTC and one MTC slice, we observed the mutual effects of slice traffic increases on performance, exposing unexpected behaviors for the traffic values at which the RACH is close to saturation. With more slices, the interaction becomes more cumbersome to predict and more complex to evaluate in detail. However, efficient bounds allow to scale the analysis up to several heterogeneous slices with limited computational power.

We have studied a cell with standard 5G configurations for what concerns the RACH and the number of service positions at the base station. With these parameters, we have shown that current technologies allow to sustain a few hundreds of HTC devices and a several thousands of MTC devices, which calls for protocol enhancements in order to scale 5G networks to more massive use cases.

References

[1] V. Mancuso, P. Castagno, M. Sereno, and M. Ajmone Marsan, "Slicing Cell Resources: The Case of HTC and MTC Coexistence," in *IEEE Conference on Computer Communications (IEEE INFOCOM 2019)*, 2019.

[2] "The NGMN alliance - at a Glance," http://www.ngmn.org, 2011.

[3] The NGMN Alliance. (2016, Jan.) Description of Network Slicing Concept. [Online]. Available: https://www.ngmn.org/uploads/media/160113_Network_Slicing_v1_0.pdf

[4] "System Architecture for the 5G System," 3GPP TS 23.501 Version 15.2.0 - Release 15, 2018. [Online]. Available: https://www.etsi.org/deliver/etsi_ts/123500_123599/123501/15.02.00_60/ts_123501v150200p.pdf

[5] P. Castagno, V. Mancuso, M. Sereno, and M. Ajmone Marsan, "A Simple Model of MTC in Smart Factories," in *IEEE Conference on Computer Communications (IEEE INFOCOM 2018)*, 2018.

[6] M. B. Shahab, R. Abbas, M. Shirvanimoghaddam, and S. J. Johnson, "Grant-Free Non-Orthogonal Multiple Access for IoT: A Survey," *IEEE Communications Surveys Tutorials*, vol. 22, no. 3, pp. 1805–1838, 2020.

[7] S. Ali, N. Rajatheva, and W. Saad, "Fast Uplink Grant for Machine Type Communications: Challenges and Opportunities," *IEEE Communications Magazine*, vol. 57, no. 3, pp. 97–103, 2019.

[8] "Technical Specification Group Radio Access Network; Study on RAN Improvements for Machine-type Communications," 3GPP, TR 37.868 Release 11, 2011.

[9] F. Baskett, K. M. Chandy, R. R. Muntz, and F. G. Palacios, "Open, Closed, and Mixed Networks of Queues with Different Classes of Customers," *J. ACM*, vol. 22, no. 2, pp. 248–260, Apr. 1975.

[10] G. Ciardo *et al.*, "Logical and Stochastic Modeling with Smart," in *Computer Performance Evaluation. Modelling Techniques and Tools*. Springer, Berlin, 2003, pp. 78–97.

[11] M. Sereno, "Computational Algorithms for Product-form of Competing Markov Chains," in *Proc. of the 10-th International Workshop on Petri Nets and Performance Models (PNPM '03)*, 2003.

[12] K. Samdanis *et al.*, "5G Network Slicing - Part 1: Concepts, Principles, and Architectures," *IEEE Communications Magazine*, vol. 55, no. 5, pp. 70–71, 2017.

[13] ——, "5G Network Slicing - Part 2: Algorithms and Practice," *IEEE Communications Magazine*, vol. 55, no. 5, pp. 110–111, 2017.

[14] D. Bega *et al.*, "AZTEC: Anticipatory Capacity Allocation for Zero-Touch Network Slicing," in *in Proc. of IEEE INFOCOM*, 2020.

[15] P. Caballero *et al.*, "Network Slicing Games: Enabling Customization in Multi-tenant Networks," in *in Proc. of IEEE INFOCOM*, 2017.

[16] T. Guo and A. Surez, "Enabling 5G RAN Slicing with EDF Slice Scheduling," *IEEE Transactions on Vehicular Technology*, vol. 68, no. 3, pp. 2865–2877, March 2019.

[17] P. Caballero *et al.*, "Multi-Tenant Radio Access Network Slicing: Statistical Multiplexing of Spatial Loads," *IEEE/ACM Transactions on Networking*, vol. 25, no. 5, pp. 3044–3058, 2017.

[18] M. Pagin *et al.*, "Enabling RAN Slicing Through Carrier Aggregation in mmWave Cellular Networks," in *in Proc. of MedComNet*, 2020.

[19] S. D'Oro *et al.*, "The Slice is Served: Enforcing Radio Access Network Slicing in Virtualized 5G Systems," in *in Proc. of IEEE INFOCOM*, 2019.

[20] J. Martn Prez *et al.*, "OKpi: All-KPI Network Slicing Through Efficient Resource Allocation," in *in Proc. of IEEE INFOCOM*, 2020.

[21] X. Li *et al.*, "5G-Crosshaul Network Slicing: Enabling Multi-Tenancy in Mobile Transport Networks," *IEEE Communications Magazine*, vol. 55, no. 8, pp. 128–137, 2017.

[22] C. Casetti *et al.*, "Network Slices for Vertical Industries," in *Proc. of IEEE Wireless Communications and Networking Conference Workshops (WCNCW)*, 2018, pp. 254–259.

[23] F. Z. Yousaf *et al.*, "Network Slicing with Flexible Mobility and QoS/QoE Support for 5G Networks," in *Proc. of IEEE International Conference on Communications Workshops (ICC Workshops)*, 2017, pp. 1195–1201.

[24] P. C. Garces *et al.*, "RMSC: A Cell Slicing Controller for Virtualized Multi-Tenant Mobile Networks," in *Proc. of IEEE 81st VTC Spring*, 2015, pp. 1–6.

[25] S. E. Elayoubi, S. B. Jemaa, Z. Altman, and A. Galindo-Serrano, "5G RAN Slicing for Verticals: Enablers and Challenges," *IEEE Communications Magazine*, vol. 57, no. 1, pp. 28–34, January 2019.

[26] Y. Hua, R. Li, Z. Zhao, X. Chen, and H. Zhang, "GAN-powered Deep Distributional Reinforcement Learning for Resource Management in Network Slicing," *IEEE Journal on Selected Areas in Communications*, pp. 1–1, 2019.

[27] C. Y. Chang *et al.*, "Radio Access Network Resource Slicing for Flexible Service Execution," in *IEEE INFOCOM WKSHPS*, 2018, pp. 668–673.

[28] Y. L. Lee *et al.*, "Dynamic Network Slicing for Multitenant Heterogeneous Cloud Radio Access Networks," *IEEE Transactions on Wireless Communications*, vol. 17, no. 4, pp. 2146–2161, 2018.

[29] S. Barmpounakis, N. Maroulis, M. Papadakis, G. Tsiatsios, D. Soukaras, and N. Alonistioti, "Network slicing - enabled RAN Management for 5G: Cross Layer Control Based on SDN and SDR," *Computer Networks*, vol. 166, p. 106987, 2020. [Online]. Available: http://www.sciencedirect.com/science/article/pii/S1389128619309776

[30] D. Bega *et al.*, "Optimising 5G Infrastructure Markets: The Business of Network Slicing," in *in Proc. of IEEE INFOCOM*, 2017.

[31] J. Zheng *et al.*, "Statistical Multiplexing and Traffic Shaping Games for Network Slicing," in *15th WiOpt*, 2017, pp. 1–8.

[32] D. Nojima *et al.*, "Resource Isolation in RAN Part While Utilizing Ordinary Scheduling Algorithm for Network Slicing," in *Proc. of IEEE 87st Vehicular Technology Conference (VTC Spring)*, 2018, pp. 1–6.

Vincenzo Mancuso is Research Associate Professor at IMDEA Networks, Madrid, Spain, and recipient of a Ramon y Cajal research grant of the Spanish Ministry of Science and Innovation. Previously, he was with INRIA (France), Rice University (USA) and University of Palermo (Italy), from where he obtained his Ph.D. in 2005. His research focus is on analysis, design, and experimental evaluation of opportunistic wireless architectures and mobile broadband services.

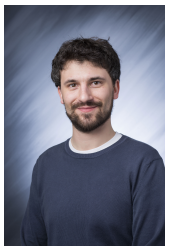

Paolo Castagno is a Post-Doctoral researcher at the Computer Science Department, University of Torino, Italy. He received his Master and Ph.D. degrees from the University of Torino, in 2014 and 2018, respectively. His research focus is on performance evaluation of computer systems and communication networks, with a specific interest on wireless networks.

Matteo Sereno was born in Nocera Inferiore, Italy. He received the Laurea degree in Computer Science from the University of Salerno, in 1987 and the Ph.D. degree in Computer Science from the University of Torino, in 1992. He is currently Full Professor at the Computer Science Department, University of Torino. His current research interests are in the area of performance evaluation of computer systems, communication networks, peer-to-peer systems, compressive sensing and coding techniques in distributed applications, game theory, queueing networks, and stochastic Petri net models.

Marco Ajmone Marsan is full professor at the Electronics and Telecommunications Department of the Politecnico di Torino in Italy, and part-time research professor at IMDEA Networks Institute in Leganes, Spain. He obtained degrees in EE from the Politecnico di Torino in 1974 and the University of California, Los Angeles (UCLA) in 1978. He received a honorary doctoral degree from the Budapest University of Technology and Economics in 2002. Since 1974 he has been at Politecnico di Torino, in the different roles of an academic career, with an interruption from 1987 to 1990, when he was a full professor at the Computer Science Department of the University of Milan. Marco Ajmone Marsan has been doing research in the fields of digital transmission, distributed systems and networking. He has been a member of the editorial board and of the steering committee of the ACM/IEEE Transactions on Networking. He is a member of the editorial boards of the journals Computer Networksand Performance Evaluationof Elsevier, and of the ACM Transactions on Modeling and Performance Evaluation of Computer Systems. He served in the organizing committee of several leading networking conferences, and he was general chair of INFOCOM 2013. Marco Ajmone Marsan is a Fellow of the IEEE, a member of the Academy of Sciences of Torino, and a member of Academia Europaea.